Hindawi Publishing Corporation
Journal of Nanomaterials
Volume 2016, Article ID 1278393, 9 pages
http://dx.doi.org/10.1155/2016/1278393

Research Article

Particle Size Dependent Photodynamic Anticancer Activity of Hematoporphyrin-Conjugated Fe_3O_4 Particles

Ki Chang Nam,[1] Kyong-Hoon Choi,[2] Kyu-Dong Lee,[3] Jung Hyun Kim,[4] Jin-Seung Jung,[3] and Bong Joo Park[2,4]

[1]*Department of Medical Engineering, Dongguk University College of Medicine, 32 Dongguk-ro, Goyang-si, Gyeonggi-do 410-820, Republic of Korea*
[2]*Plasma Bioscience Research Center, Kwangwoon University, 20 Kwangwoongil, Nowon-gu, Seoul 139-701, Republic of Korea*
[3]*Department of Chemistry, Gangneung-Wonju National University, 7 Jukheon-gil, Gangneung-si, Gangwon-do 210-702, Republic of Korea*
[4]*Department of Electrical & Biological Physics, Kwangwoon University, 20 Kwangwoongil, Nowon-gu, Seoul 139-701, Republic of Korea*

Correspondence should be addressed to Jin-Seung Jung; jjscm@gwnu.ac.kr and Bong Joo Park; parkbj@kw.ac.kr

Received 22 October 2015; Accepted 14 December 2015

Academic Editor: Marinella Striccoli

Nanomedicine, which involves the use of magnetic nanoparticles such as Fe_3O_4, has provided novel technical solutions for cancer diagnosis and treatment. Most studies in nanomedicine have focused on the use of nanoparticles with magnetic resonance imaging and hyperthermia. However, to achieve optimum anticancer effects, it is important to understand the physicochemical properties of magnetic nanoparticles and their interactions with biological entities. In this study, we synthesized Fe_3O_4 particles of various sizes and conjugated them with hematoporphyrin (HP) molecules by using a simple surface-modification method. HP molecules were covalently bound to the surface of Fe_3O_4 particles by a wet chemical process, resulting in Fe_3O_4@HPs particles that were uniform in size, were nontoxic, and exhibited strong anticancer effects on human prostate cancer (PC-3) and breast cancer (MDA-MB-231) cell lines. The Fe_3O_4@HPs particles showed remarkable and efficient photodynamic anticancer activity, depending on their particle size. These results indicate that all size of Fe_3O_4@HPs particles can be useful for photodynamic anticancer therapy, although the smaller size is better than the larger size and further studies will be needed to confirm the potential for clinical anticancer treatment.

1. Introduction

Recent progress in nanomedicine has led to the development of magnetic nanoparticles that show great potential for application in early diagnosis, targeted therapy, and personalized medicine [1–5]. In particular, efforts have been focused on early and accurate diagnosis and effective treatment. However, the results from preclinical and clinical studies of magnetic nanoparticles indicate several serious limitations such as inability to evade the immune system, anticipate toxicity via interactions with biological entities such as proteins and cell membranes, and achieve optimal bioperformance [6, 7].

To overcome these limitations, various approaches based on the functionalized surface coating of nanoparticles have been attempted to improve clinical outcome. Saito et al. [8] prepared dextran that is, ferucarbotran-coated magnetic nanoparticles, for use as enhanced contrast reagents in magnetic resonance imaging. Kievit et al. [9] proposed a facial approach to prepare specific, functional PEI-PEG-chitosan modified magnetic nanoparticles for a nonviral nanoparticle gene carrier system. Moreover, Mahmoudi et al. [10] fabricated polyethylene glycol fumarate-coated magnetic nanoparticles for bioimaging and drug delivery. In addition to polymeric coating, inorganic coating of magnetic nanoparticles with silica or gold has attracted attention, with regard to further surface derivatization of nanoparticles and because of their influence on colloidal stability and the biological behavior of magnetic nanoparticles in biomedical applications [11, 12]. Particularly, these coated nanoparticles

can be easily surface-functionalized for bioconjugation to antibodies and for targeted delivery with particle localization in a specific area [13–16]. Although various studies have reported a more efficient surface modification of magnetic nanoparticles, little work has been undertaken in this regard to systematically compare the size-dependent photodynamic anticancer efficiency among photosensitizer-coated magnetic nanoparticles. Among various photosensitizers, HP, a major biomolecule in erythrocytes, is enriched in tumor regions and can kill cancer cells by generating reactive oxygen species [17]. Therefore, HP-coated magnetic particles may be quite promising for applications in versatile imaging diagnosis and photodynamic therapy (PDT).

In this study, we primarily focused on comparing the photodynamic anticancer efficiencies of Fe_3O_4@HPs with various particle sizes. For this purpose, biocompatible Fe_3O_4@HPs of well-defined sizes were fabricated by a simple surface-modification process that functionalizes Fe_3O_4 particles by coating them with HP to allow the killing of cancer cells. The photodynamic anticancer activities of Fe_3O_4@HPs were evaluated with human prostate cancer (PC-3 cell) and breast cancer (MDA-MB-231 cell) cell lines *in vitro* to confirm the anticancer efficacy for clinical application.

2. Materials and Methods

All chemical reagents were of analytical grade and used as received without further purification.

2.1. Synthesis of Fe_3O_4 Particles of Different Sizes. Fe_3O_4 particles of different sizes were prepared as previously described [18]. Briefly, 0.54 g $FeCl_3{\cdot}6H_2O$ and 1.5 g NaOAc were dissolved in 20 mL ethylene glycol (EG) and diethylene glycol (DEG) mixture solvent, and the mixture was vigorously stirred for 30 min. The solution was transferred to an 80 mL, Teflon-lined autoclave, which was sealed, and the temperature was maintained at 200°C for 10 h, after which the solution was cooled to room temperature (RT) naturally. The black precipitate formed was collected by magnetic decantation, washed with deionized water and absolute alcohol several times, and then dried in a vacuum oven at 60°C for 6 h. The volume ratio of EG/DEG (V_{EG}/V_{DEG}) determined the size of the Fe_3O_4 particles; thus, we obtained Fe_3O_4 particles with average sizes of 92.7, 171.9, 259.9, and 404.5 nm by using V_{EG}/V_{DEG} ratios of 5/15, 10/10, 15/5, and 20/0, respectively.

2.2. Synthesis of Fe_3O_4@HPs Particles. To conjugate photosensitizer (PS) molecules, the surface of Fe_3O_4 particles of each size was treated with dielectric barrier discharge plasma for 30 min, as previously reported [19].

Fe_3O_4@HPs particles were prepared by a wet chemical process, as previously described [20]. The resulting Fe_3O_4 particles in tetrahydrofuran (THF) (20 mg/mL, 5 mL THF) were mixed with a solution of HP/THF (2.02×10^{-4} M). The mixture was agitated at RT for 24 h. After the reaction was complete, the product was washed with THF solvent several times. After the final wash, the residual THF solvent was removed and the particles were dried at 60°C for 6 h.

2.3. Characterization of Fe_3O_4@HPs Particles. Field emission scanning electron microscopy (FESEM) was performed using a Hitachi SU-70 scanning electron microscope equipped with an energy-dispersive X-ray spectroscope (EDS). X-ray diffraction (XRD) pattern of the product was obtained using a PANalytical Pert Pro MPD X-ray diffractometer with a Cu Kα radiation source (λ = 0.15405 nm) operated at 40 kV and 150 mA in a 2θ range of 20° to 80°. The magnetic properties of the particles were investigated using a vibrating sample magnetometer (VSM; PPMS-9T, Quantum Design). Photoluminescence (PL) and photoluminescence excitation (PLE) spectra were measured using a spectrophotometer (F-4500, Hitachi).

2.4. Detection of Singlet Oxygen. We used 1,3-diphenylisobenzofuran (DPBF), a sensitive probe of reactive oxygen species (ROS), to detect singlet oxygen ($^1O_2$), via oxidative degradation of DPBF by $^1O_2$ to produce nonabsorbent o-dibenzoylbenzene [21, 22], which resulted in a continual decrease in the absorption intensity of DPBF, as light irradiation continued. In the photochemical experiment, a 3.0075 mL aliquot of THF solution containing Fe_3O_4@HPs particles and DPBF (4.61×10^{-8} M) was introduced into a 1 cm quartz cell in the dark. The experiments were carried out by irradiating the samples with a Xe lamp (150 W, Abet Technologies, USA). A 480 nm, glass cutoff filter was used to filter out ultraviolet light. Photodegradation of DPBF was monitored by recording optical density (OD) of the absorption peak at 424 nm. After every 10 min of irradiation, the absorption spectrum of the samples was monitored using a UV-Vis spectrophotometer. A comparison was made between DPBF photodegradation of Fe_3O_4@HPs particles of different sizes to evaluate the relative capacity for $^1O_2$ production.

2.5. Biocompatibility Assessment. To confirm the biocompatibility of Fe_3O_4@HPs particles, cytotoxicity tests were performed with fibroblasts (L-929 cells), prostate cancer (PC-3), and breast cancer (MDA-MB-231) cells, as previously described [19, 20, 23, 24]. Briefly, precultured cells were plated in a 24-well plate at 2.0×10^5 cells/mL for L-929, at 1.0×10^5 cells/mL for PC-3, and MDA-MB-231 cells. The cells were cultured at 37°C in an atmosphere containing 5% CO_2 for 24 h and then incubated with different concentrations (0, 6.25, 12.5, 25, and 50 μg/mL) of Fe_3O_4@HPs particles at 37°C in an atmosphere containing 5% CO_2 for another 24 h in the dark. Viability of each cell line was evaluated using cell counting kit-8 (CCK-8, Dojindo Laboratories, Kumamoto, Japan) to confirm the biocompatibility of Fe_3O_4@HPs particles. The relative cell viability was calculated as percentage survival in relation to untreated control cells.

2.6. Photodynamic Anticancer Activity Assessment. In vitro photodynamic anticancer activities of Fe_3O_4@HPs particles of different sizes were evaluated on PC-3 and MDA-MB-231 cells, as previously reported [19, 20, 23, 24]. Each cell line was incubated with different concentrations (0, 6.25, 12.5, 25, 50, and 100 μg/mL) and different sizes of Fe_3O_4@HPs particles at

37°C in an atmosphere containing 5% CO_2 for 2 h in the dark. After replenishing the medium, the cells were irradiated by a conventional, green-light-emitting diode (LED). Twenty-four LEDs of type FD-32G-N1-1 (Shenzhen Fedy Technology Co., China) were used for building of the PDT-mode of the system developed, with total electrical power 3 W at 505 nm maximum wavelength and power density up to 7 mW/cm^2 (maximum). After irradiation, the cells were incubated for another 24 h and, on the following day, cell viability was determined using a CCK-8 kit to measure photokilling activity on the cancer cells.

2.7. Morphological Detection of Apoptotic Cell Death. To evaluate apoptotic cell death, cell membrane translocation of PC-3 cells was analyzed using an EzWay Annexin V-fluorescein isothiocyanate (Annexin V-FITC) apoptosis detection kit (K29100, Komabiotech Inc., Seoul, Republic of Korea), according to the manufacturer instructions and as previously described [19]. Briefly, the PC-3 cells were incubated for 2 h after LED irradiation, rinsed with phosphate-buffered saline (PBS) and binding buffer, and stained with Annexin V-FITC reagent for 15 min at RT in the dark to stain the cell membrane. After incubation, the cells were washed with cold binding buffer and stained with propidium iodide (PI) to stain the nuclei.

To confirm nuclear fragmentation, PC-3 cells were irradiated with LED, fixed in ice-cold 70% ethanol for 15 min, and dried at RT. Cell membrane was stained with Texas Red C2-maleimide (30 ng/mL in PBS) for 2 h, and cell nuclei were counterstained with Hoechst 33342 (1 μg/mL in PBS) for 10 min.

Images of cells stained with fluorescent dyes were captured using a laser scanning confocal microscope (LSM 700) with a 20x objective lens and fluorescence optics (excitation at 488 nm for FITC, 530 nm for PI, 595 nm for Texas Red C2-maleimide, and 352 nm for Hoechst 33342; emission at 518 nm for FITC, 615 nm for Texas Red C2-maleimide, and 620 nm for PI). All images were analyzed using ZEN imaging software (ZEN 2009, Carl Zeiss MicroImaging GmbH).

2.8. Statistical Analysis. Data were obtained from three independent experiments ($n = 6$). Quantitative data are expressed as mean ± standard deviation (SD), and statistical comparisons were carried out using Student's t-test. Significant differences were indicated by $p < 0.05$.

3. Results and Discussion

EG is an effective reaction medium for the fabrication of fine metal or metal oxide particles owing to its high solubility and reducibility [25, 26]. When DEG is introduced together with EG in the reaction system, the size of the Fe_3O_4 particles can be successfully reduced by only varying the V_{EG}/V_{DEG} ratio [27]. Similarly, we obtained Fe_3O_4 particles of different sizes by adjusting the V_{EG}/V_{DEG} ratio of the synthetic solvent. FE-SEM images were captured to examine the morphology and size of the resulting spherical particles, as shown in Figures 1(a)–1(d). All particles were spherical and remarkably uniform. In general, the size of as-prepared external particles can be precisely adjusted to obtain particles ranging between 93 and 405 nm in size. When the V_{EG}/V_{DEG} ratios in this study were varied from 5/15 to 10/10, 15/5, and 7/0, the diameters of the resulting Fe_3O_4 particles were 92.7, 171.9, 259.9, and 404.5 nm, respectively. These results indicate that the mean diameter of the prepared Fe_3O_4 particles is proportional to the V_{EG}/V_{DEG} ratios used during the solvothermal reaction. As shown in Figure 1 inset, the FE-SEM image at high magnification shows that the individual spheres were composed of irregular nanograins, measuring 10 to 25 nm in size. Figures 1(e)–1(h) show size histograms of the Fe_3O_4 particles with various sizes, which were estimated by sampling 300 particles in different regions of the SEM image. These data show the mean particle size and size distribution, where the average diameters $\langle\varphi\rangle$ = 92.7, 171.9, 259.9, 404.5 with σ = 12.3, 16.3, 18.6, 11.8 were obtained, respectively, using a Gaussian fit.

The crystalline structures of the as-prepared Fe_3O_4 particles were characterized by XRD analysis, as shown in Figure 2. The position and relative intensity of all diffraction peaks matched well with the face-center cubic spinel structure of Fe_3O_4 (JCPDS card number: 19-0629). These results indicate that the peaks become sharper with increase in crystallite size. According to the Scherrer formula, the average crystallite sizes calculated were approximately 8.5, 11.7, 15.7, and 26.2 nm, based on the strongest peaks (311), and were much smaller than the external diameters (93 to 405 nm) of the Fe_3O_4 particles. These results suggest that the grain size of Fe_3O_4 particle shows a gradual increase with an increasing volume ratio of EG. Therefore, the volume ratio of EG/DEG plays an important role in determining the particle size and grain size.

The size-dependent magnetic properties of Fe_3O_4 particles were measured at RT, and the magnetization curves are shown in Figure 3. All the magnetization curves display relatively high saturation of magnetization (M_s). The M_s values of Fe_3O_4 particles with sizes of 92.7, 171.9, 259.9, and 404.5 nm were 60.1, 69.9, 79.8, and 89.5 emu/g, respectively. All the as-prepared samples possessed an M_s value relatively smaller than those of bulk Fe_3O_4 particles. The magnetic remnant M_r and coercivity H_c showed a significant increase with increasing particle size, indicating the transformation from superparamagnetic to ferromagnetic nature. This result can be ascribed to the sequentially increased primary nanocrystal size.

The size-controlled Fe_3O_4 particles can be easily bonded with HP molecules after plasma treatment by means of the surface-modification process. The photoluminescence excitation (PLE) spectrum of Fe_3O_4@HPs showed the same characteristics as that of pure HP in THF solvent, showing an absorbance peak at 400 nm, which is the Soret band of PS, and the Q bands were located at 500, 532, and 574 nm, as shown in Figure 4. At the excitation wavelength of 500 nm, pure HP produced two strong emission peaks at 631 and 695 nm, whereas Fe_3O_4@HPs provided slightly red-shifted peaks at 649 and 697 nm. This result implies that the HP molecules were immobilized onto the size-controlled Fe_3O_4 particle surface.

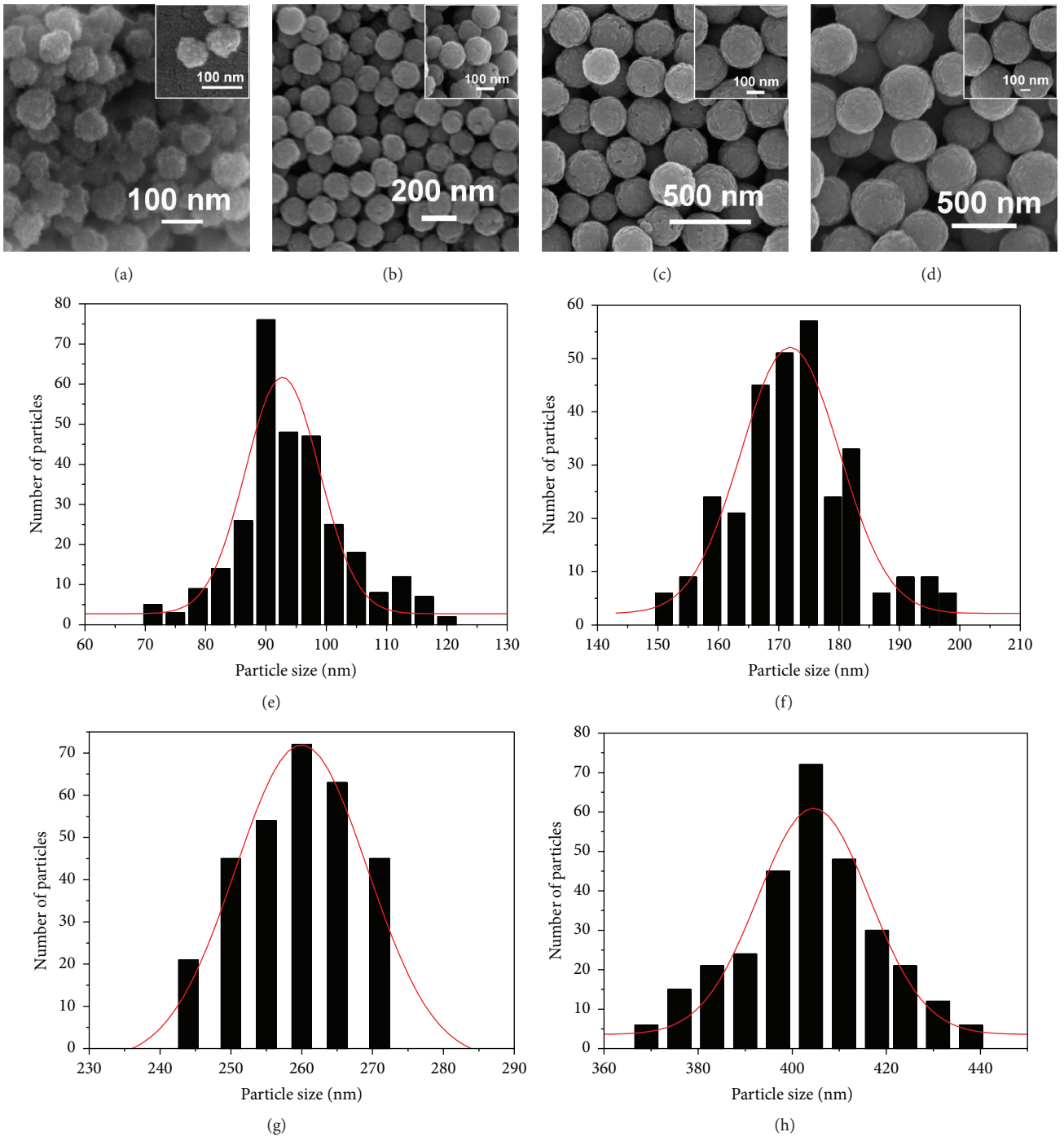

FIGURE 1: FE-SEM images of the size-controlled Fe_3O_4 particles synthesized using different ratios of V_{EG}/V_{DEG}: (a) 5/15, (b) 10/10, (c) 15/5, and (d) 20/0, with other experimental parameters kept constant; (e) to (h) histograms of particle-size distributions of the size-controlled Fe_3O_4 particles.

The HP loading content of the hybrid Fe_3O_4@HPs particles depends on the weight and size of the Fe_3O_4 particles as a substrate. As the size of the particle decreases, the number of HP molecules bonded to the surfaces of the Fe_3O_4 particle increases at the same weight condition, owing to the increase in the surface area of the whole particles. Under the same weight condition (50 μg Fe_3O_4@HPs particles), the HP contents observed were 2.03, 1.88, 1.81, and 1.46 μg, according to the various particle sizes (from 92.7 to 404.5 nm). These results were confirmed by the analysis of UV-VIS absorption spectra of the size-controlled Fe_3O_4@HPs particles compared with the standard calibration. Therefore, the smallest nanoparticle complex is expected to represent the highest generation efficiency of singlet oxygen, with increase in dose.

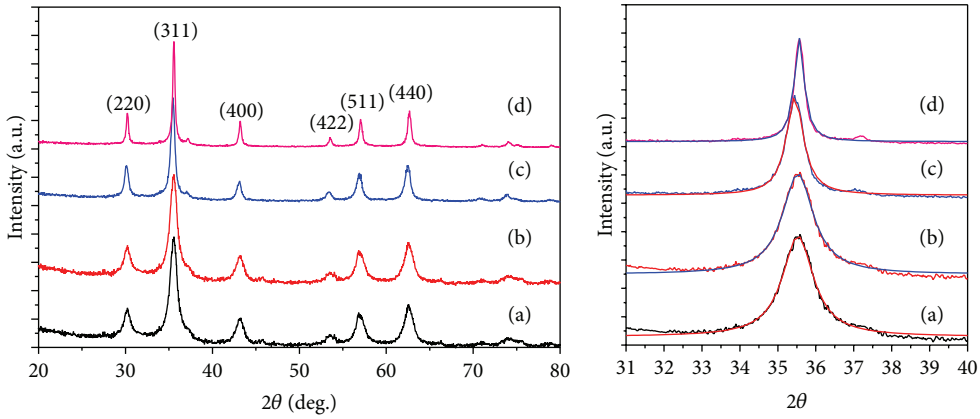

	V_{EG}/V_{DEG}	Grain size (nm)
(a)	5/15	8.5
(b)	10/10	11.7
(c)	15/5	15.7
(d)	20/0	26.2

FIGURE 2: XRD patterns of the size-controlled Fe_3O_4 particles synthesized using different ratios of V_{EG}/V_{DEG}: (a) 5/15, (b) 10/10, (c) 15/5, and (d) 20/0.

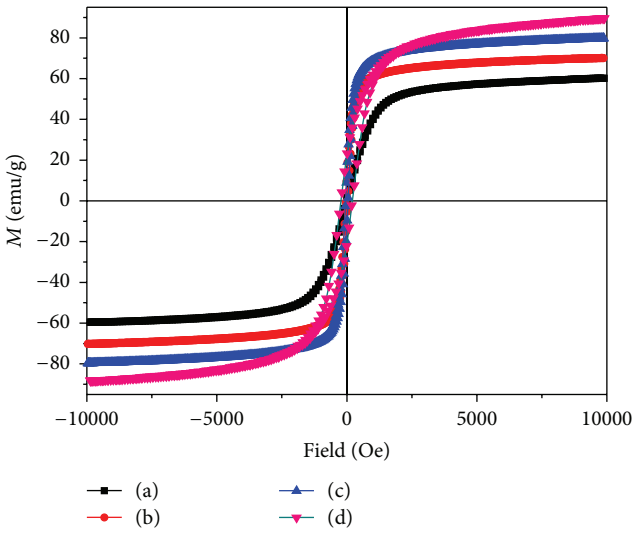

FIGURE 3: Room temperature magnetic hysteresis loops of the size-controlled Fe_3O_4 particles synthesized using different ratios of V_{EG}/V_{DEG}: (a) 5/15, (b) 10/10, (c) 15/5, and (d) 20/0.

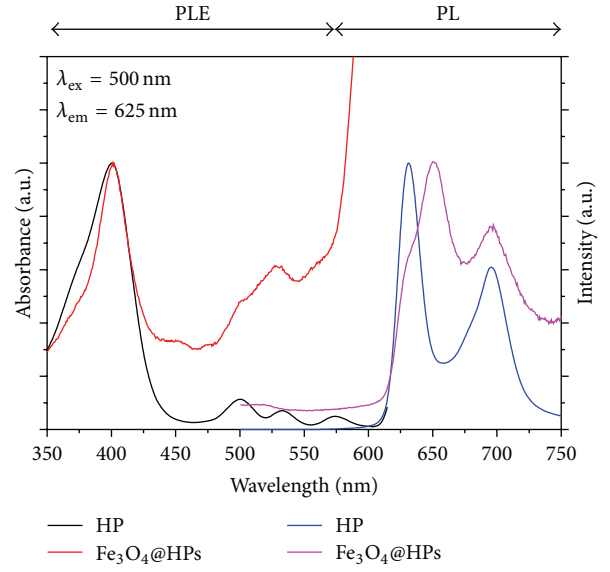

FIGURE 4: PL and PLE spectra of pure HP and Fe_3O_4@HPs in THF. Excitation and detection wavelengths used were 500 and 625 nm, respectively, for both PL and PLE spectra.

Singlet oxygen ($^1O_2$) generation from the Fe_3O_4@HPs was confirmed by indirect detection of DPBF photodegradation. When the Fe_3O_4@HPs particles are excited by light, they emit phosphorescence as a form of deexcitation and they can achieve an intersystem cross, producing $^1O_2$ (excited state of O_2) by transferring energy to the surrounding oxygen molecules, as another form of deexcitation. DPBF, as a $^1O_2$ probe, has a typical absorption band at 424 nm. As shown in Figure 5, the absorption intensity of DPBF in all Fe_3O_4@HPs solutions decreased with the light irradiation time and the particle size of Fe_3O_4@HPs. The degradation rate was proportional to the $^1O_2$ yield. These results indicate that the photodegradation efficiency of DPBF was increased as the particle size of Fe_3O_4@HPs decreased to 404.5, 259.9, 171.9, and 92.7 nm, respectively. These results are consistent with the number of HP molecules conjugated on each particle with decrease in particle size.

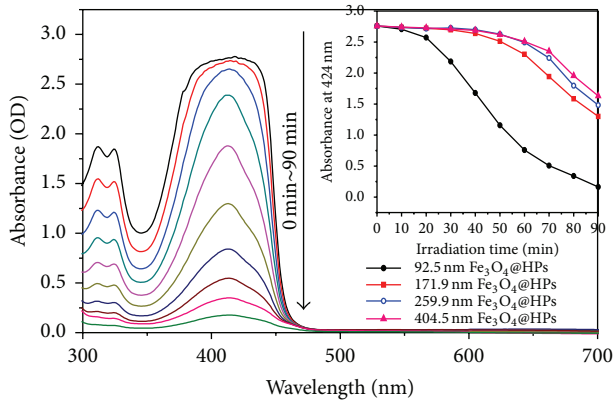

FIGURE 5: Irradiation time-dependent UV-Vis spectra of DPBF in THF solution with the Fe_3O_4@HPs, excited using a Xe lamp. Inset represents the absorption OD of DPBF in THF at 424 nm with Fe_3O_4@HPs as a function of irradiation time.

To confirm the biocompatibility of each size of Fe_3O_4@HPs, we used fibroblasts (L-929) and two cancer cell lines (PC-3 and MDA-MB-231) to check cytotoxic effects of the nanoparticles under dark conditions, using the method recommended by the International Organization for Standardization (ISO) 10993-5 [28].

In the cytotoxicity test, cell viability with all particle sizes was > 90%, as shown in Figure 6. This result indicates that the Fe_3O_4@HPs are biocompatible, without exhibiting any cytotoxicity, and they can be safely used clinically as anticancer therapy.

To confirm the photodynamic anticancer activities of Fe_3O_4@HPs depending on the particle size, we used two cancer cell lines (prostate cancer PC-3 cells and breast cancer MDA-MB-231 cells). Photodynamic anticancer activities were evaluated by the CCK-8 method after irradiation with LED, as shown in Figure 7.

Cell viability of prostate cancer cells with 95 nm Fe_3O_4@HPs was 0.6% ($p < 0.002$) for 100 μg/mL, 0.8% ($p < 0.003$) for 50 μg/mL, and 13.2% ($p < 0.007$) for 25 μg/mL. On the other hand, values for PC-3 cells with 175 nm, 280 nm, and 420 nm Fe_3O_4@HPs particle sizes were 2.0%, 1.8%, and 1.9% for 100 μg/mL; 8.9%, 9.2%, and 15.7% for 50 μg/mL; and 31.4%, 37.9%, and 61.4% for 25 μg/mL, respectively. These data indicate that the values for photodynamic anticancer activity for PC-3 cells were 98.1%, 99.2%, and 86.8% with 95 nm Fe_3O_4@HPs; 98.0%, 89.1%, and 68.4% with 175 nm Fe_3O_4@HPs; 98.2%, 90.8%, and 62.1% with 280 nm Fe_3O_4@HPs; and 90.1%, 84.3%, and 38.6% with 420 nm Fe_3O_4@HPs, respectively.

Additionally, the photodynamic anticancer activity values for breast cancer (MDA-MB-231) cells were 97.3%, 93.0%, and 73.0% with 95 nm Fe_3O_4@HPs; 93.9%, 87.9%, and 75.7% with 175 nm Fe_3O_4@HPs; 85.7%, 84.2%, and 78.0% with 280 nm Fe_3O_4@HPs; and 75.5%, 66.3%, and 43.6% with 420 nm Fe_3O_4@HPs, respectively.

These results are consistent with the amount of HP on the surface of each size of the Fe_3O_4@HPs, as described above. A large quantity of HP on the Fe_3O_4@HPs surface can lead to the generation of a large quantity of singlet oxygen, which plays a key role as a mediator of cell death during light irradiation, and the singlet oxygen generated from Fe_3O_4@HPs could determine not only the photodynamic anticancer effects but also the type of cell death [19, 29].

From these results, we confirmed that various sizes of the Fe_3O_4@HPs nanoparticles exerted a dose-dependent photodynamic anticancer activity in both cancer cells tested. Additionally, the Fe_3O_4@HPs showed slightly greater photokilling efficacy against prostate cancer cells as compared to breast cancer cells, suggesting that there is a correlation in photokilling efficacy between particle sizes and cell types.

We also observed cell membrane translocation and nuclear fragmentation of cancer cells while confirming apoptotic cell death, using an Annexin V-FITC apoptosis detection kit and a fluorescence dye, Hoechst 33342, as cell membrane translocation and nuclear fragmentation of cells are hallmarks of apoptotic cell death. These methods can be used to easily detect apoptotic cell death, as Annexin V-FITC binds to the translocated membrane phosphatidylserine, while nuclear deformation and fragmentation is visualized by staining with PI and Hoechst 33342.

Figure 8 shows cell membrane translocation and nuclear fragmentation of PC-3 cells. In Figure 8(a), the images treated with the Fe_3O_4@HPs show early and late-stage apoptotic cell death after irradiation by emitting green fluorescence indicating cell membrane translocation and red fluorescence marking nuclear material. However, the control cells stained by both dyes, Annexin V-FITC and PI, did not show fluorescence, demonstrating that cancer cell death by light irradiation after treatment of Fe_3O_4@HPs may occur by means of apoptosis for all sizes of Fe_3O_4@HPs nanoparticles.

Furthermore, we also confirmed nuclear fragmentation in PC-3 cells using Hoechst 33342 fluorescence dye as shown in Figure 8(b). The images of Fe_3O_4@HPs-treated PC-3 cells show fragmented nuclear material with a reduced and granular nuclear body (line arrows) regardless of particle size, as compared with the control.

From these results, we confirmed that the photodynamic anticancer activities of Fe_3O_4@HPs with various particle sizes may occur via apoptotic cell death after light irradiation and

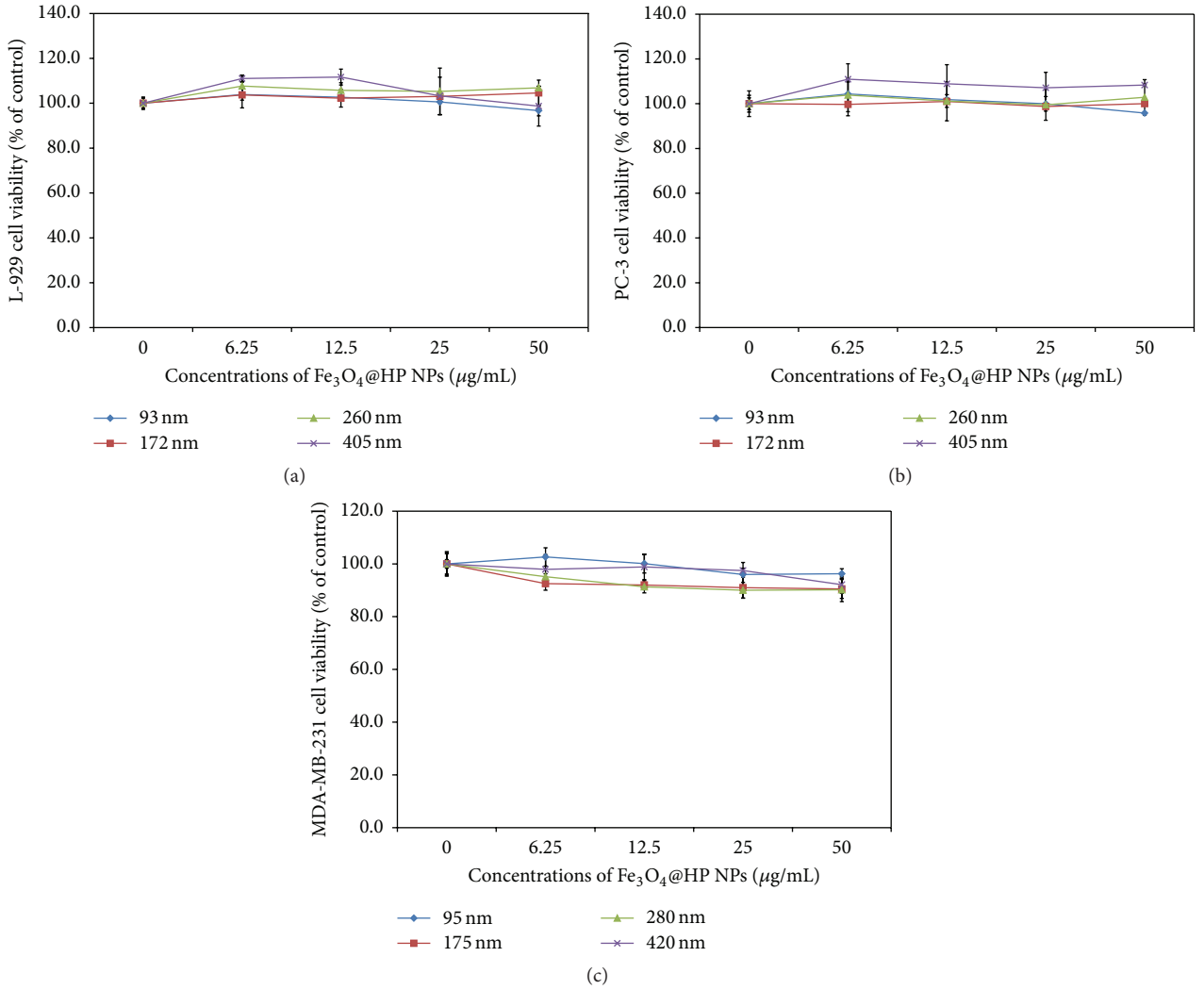

FIGURE 6: Cytotoxicities of Fe_3O_4@HPs particles against fibroblasts and cancer cells. (a) Fibroblasts (L-929 cells), (b) prostate cancer cells (PC-3 cells), and (c) breast cancer cells (MDA-MB-231 cells). Data are expressed as a mean ± standard deviation ($n = 6$) and analyzed by Student's t-tests. Statistical significance was considered at $p < 0.05$.

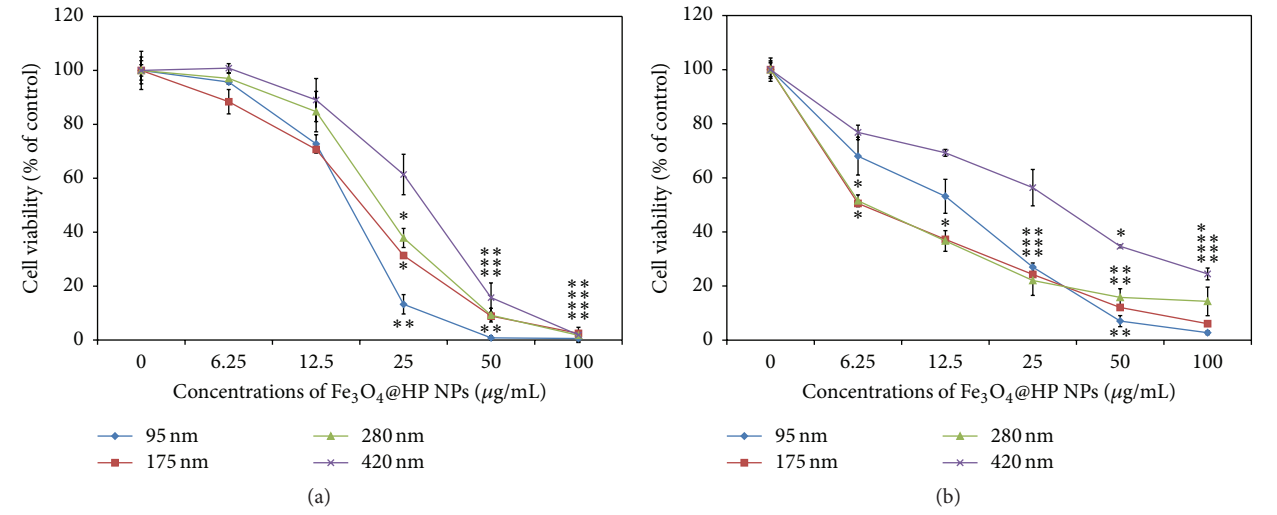

FIGURE 7: Photodynamic anticancer activities of Fe_3O_4@HPs particles. Viability of (a) prostate cancer cells (PC-3 cells) and (b) breast cancer cells (MDA-MB-231 cells). Cells were incubated with various concentrations of Fe_3O_4@HPs particles for 2 h in the dark, prior to LED irradiation for 30 min. Data are expressed as a mean ± standard deviation ($n = 6$) and analyzed by Student's t-tests. Statistical significance was considered at $p < 0.05$. ($^{*}p < 0.05$, $^{**}p < 0.005$ versus control).

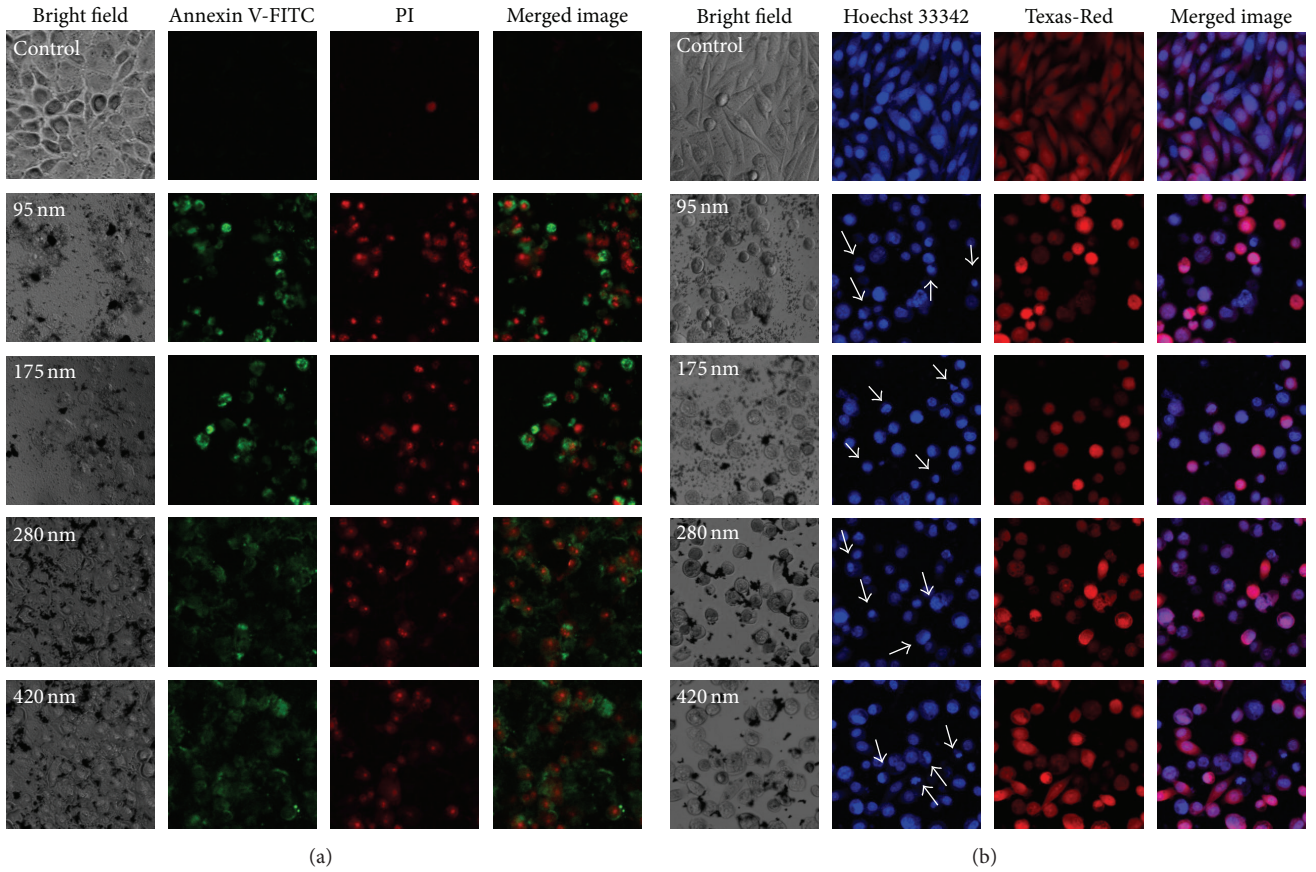

Figure 8: Confocal fluorescence images of cell membrane translocation and nuclear fragmentation in PC-3 cells. (a) Confocal fluorescence images of cell membrane translocation in PC-3 cells stained with Annexin V-FITC (green) for cell membrane and PI (red) for nucleus, after irradiation for 30 min. (b) Confocal fluorescence images of nuclear fragmentation (line arrows) in PC-3 cells stained with Hoechst 33342 (blue) for nucleus and Texas-Red (red) for whole cells. Apoptosis was induced by irradiation for 30 min after treatment with 25 μg/mL of 92.7 nm Fe_3O_4@HPs particles for 2 h.

the Fe_3O_4@HPs with various particle sizes can be useful for PDT after confirming the efficacy of anticancer activity *in vivo*.

4. Conclusions

In this study, multifunctional Fe_3O_4 of various particle sizes were fabricated and used as a platform for surface conjugation of HP, which exhibited photodynamic anticancer activities. These multifunctional Fe_3O_4@HPs particles showed good chemical stability and biocompatibility, as well as effective photodynamic anticancer activity when tested on prostate cancer (PC-3) and breast cancer (MDA-MB-231) cell lines. Additionally, these multifunctional Fe_3O_4@HPs particles could load varying quantities of HP molecules depending on their size.

These results indicate that all size of Fe_3O_4@HPs particles can be useful for PDT, although the smaller size is better than the larger size and further studies will be needed to confirm the potential for clinical anticancer treatment.

Conflict of Interests

The authors declare that there is no conflict of interests regarding the publication of this paper.

Authors' Contribution

Ki Chang Nam, Kyong-Hoon Choi, Kyu-Dong Lee, and Jung Hyun Kim contributed equally to this work.

Acknowledgment

This study was financially supported by a grant from the National Research Foundation of Korea (NRF-2015M3A9E2066855).

References

[1] V. Wagner, A. Dullaart, A.-K. Bock, and A. Zweck, "The emerging nanomedicine landscape," *Nature Biotechnology*, vol. 24, no. 10, pp. 1211–1217, 2006.

[2] A. Béduneau, P. Saulnier, and J.-P. Benoit, "Active targeting of brain tumors using nanocarriers," *Biomaterials*, vol. 28, no. 33, pp. 4947–4967, 2007.

[3] L. Brannon-Peppas and J. O. Blanchette, "Nanoparticle and targeted systems for cancer therapy," *Advanced Drug Delivery Reviews*, vol. 56, no. 11, pp. 1649–1659, 2004.

[4] A. G. Cuenca, H. Jiang, S. N. Hochwald, M. Delano, W. G. Cance, and S. R. Grobmyer, "Emerging implications of nanotechnology on cancer diagnostics and therapeutics," *Cancer*, vol. 107, no. 3, pp. 459–466, 2006.

[5] O. C. Farokhzad and R. Langer, "Nanomedicine: developing smarter therapeutic and diagnostic modalities," *Advanced Drug Delivery Reviews*, vol. 58, no. 14, pp. 1456–1459, 2006.

[6] B. Pelaz, G. Charron, C. Pfeiffer et al., "Interfacing engineered nanoparticles with biological systems: anticipating adverse nano-bio interactions," *Small*, vol. 9, no. 9-10, pp. 1573–1584, 2013.

[7] M. Moros, S. G. Mitchell, V. Grazúa, and J. M. de la Fuente, "The fate of nanocarriers as nanomedicines in vivo: important considerations and biological barriers to overcome," *Current Medicinal Chemistry*, vol. 20, no. 22, pp. 2759–2778, 2013.

[8] S. Saito, M. Tsugeno, D. Koto et al., "Impact of surface coating and particle size on the uptake of small and ultrasmall superparamagnetic iron oxide nanoparticles by macrophages," *International Journal of Nanomedicine*, vol. 7, pp. 5415–5421, 2012.

[9] F. M. Kievit, O. Veiseh, N. Bhattarai et al., "PEI-PEG-chitosan copolymer coated iron oxide nanoparticles for safe gene delivery: synthesis, complexation, and transfection," *Advanced Functional Materials*, vol. 19, no. 14, pp. 2244–2251, 2009.

[10] M. Mahmoudi, A. Simchi, M. Imani, and U. O. Häfeli, "Superparamagnetic iron oxide nanoparticles with rigid cross-linked polyethylene glycol fumarate coating for application in imaging and drug delivery," *The Journal of Physical Chemistry C*, vol. 113, no. 19, pp. 8124–8131, 2009.

[11] C. S. S. R. Kumar, *Magnetic Nanomaterials*, Wiley-VCH, Weinheim, Germany, 2009.

[12] K. T. Thanh Nguyen, *Magnetic Nanoparticles*, CRC Press, Taylor & Francis, Boca Raton, Fla, USA, 2012.

[13] K. L. Hultman, A. J. Raffo, A. L. Grzenda, P. E. Harris, T. R. Brown, and S. O'Brien, "Magnetic resonance imaging of major histocompatibility class II expression in the renal medulla using immunotargeted superparamagnetic iron oxide nanoparticles," *ACS Nano*, vol. 2, no. 3, pp. 477–484, 2008.

[14] A. Burns, H. Ow, and U. Wiesner, "Fluorescent core-shell silica nanoparticles: towards 'lab on a particle' architectures for nanobiotechnology," *Chemical Society Reviews*, vol. 35, no. 11, pp. 1028–1042, 2006.

[15] C.-P. Tsai, C.-Y. Chen, Y. Hung, F.-H. Chang, and C.-Y. Mou, "Monoclonal antibody-functionalized Mesoporous Silica Nanoparticles (MSN) for selective targeting breast cancer cells," *Journal of Materials Chemistry*, vol. 19, no. 32, pp. 5737–5743, 2009.

[16] Z. Zhang, Q. Sun, J. Zhong et al., "Magnetic resonance imaging-visible and pH-sensitive polymeric micelles for tumor targeted drug delivery," *Journal of Biomedical Nanotechnology*, vol. 10, no. 2, pp. 216–226, 2014.

[17] Y. Ren, R. Wang, Y. Liu et al., "A hematoporphyrin-based delivery system for drug resistance reversal and tumor ablation," *Biomaterials*, vol. 35, no. 8, pp. 2462–2470, 2014.

[18] K.-H. Choi, W.-S. Chae, E.-M. Kim et al., "A Facile fabrication of Fe_3O_4/ZnO Core-Shell submicron particles with controlled size," *IEEE Transactions on Magnetics*, vol. 47, no. 10, pp. 3369–3372, 2011.

[19] B. J. Park, K.-H. Choi, K. C. Nam et al., "Photodynamic anticancer activities of multifunctional cobalt ferrite nanoparticles in various cancer cells," *Journal of Biomedical Nanotechnology*, vol. 11, no. 2, pp. 226–235, 2015.

[20] K.-H. Choi, E.-W. Choi, J. Min et al., "Comparison study on photodynamic anticancer activity of multifunctional magnetic particles by formation of cations," *IEEE Transactions on Magnetics*, vol. 50, no. 11, Article ID 5200704, 2014.

[21] R. M. Dickson and L. A. Lyon, "Unidirectional plasmon propagation in metallic nanowires," *The Journal of Physical Chemistry B*, vol. 104, no. 26, pp. 6095–6098, 2000.

[22] X. Huang, X.-J. Tian, W.-L. Yang, B. Ehrenberg, and J.-Y. Chen, "The conjugates of gold nanorods and chlorin e6 for enhancing the fluorescence detection and photodynamic therapy of cancers," *Physical Chemistry Chemical Physics*, vol. 15, no. 38, pp. 15727–15733, 2013.

[23] K.-H. Choi, K. C. Nam, H.-J. Kim et al., "Synthesis and characterization of photo-functional magnetic nanoparticles (Fe_3O_4@HP) for applications in photodynamic cancer therapy," *Journal of the Korean Physical Society*, vol. 65, no. 10, pp. 1658–1662, 2014.

[24] B. J. Park, K. Choi, K. C. Nam et al., "Photodynamic anticancer activity of $CoFe_2O_4$ nanoparticles conjugated with hematoporphyrin," *Journal of Nanoscience and Nanotechnology*, vol. 15, no. 10, pp. 7900–7906, 2015.

[25] J. Chen, T. Herricks, M. Geissler, and Y. Xia, "Single-crystal nanowires of platinum can be synthesized by controlling the reaction rate of a polyol process," *Journal of the American Chemical Society*, vol. 126, no. 35, pp. 10854–10855, 2004.

[26] B. Jia and L. Gao, "Morphological transformation of Fe_3O_4 spherical aggregates from solid to hollow and their self-assembly under an external magnetic field," *The Journal of Physical Chemistry C*, vol. 112, no. 3, pp. 666–671, 2008.

[27] S. Xuan, F. Wang, Y.-X. J. Wang, J. C. Yu, and K. C.-F. Leung, "Facile synthesis of size-controllable monodispersed ferrite nanospheres," *Journal of Materials Chemistry*, vol. 20, no. 24, pp. 5086–5094, 2010.

[28] ISO, "Part 5: tests for *in vitro* cytotoxicity," International Standard ISO 10993-5, International Organization for Standardization, Geneva, Switzerland, 2009.

[29] J. Yamamoto, S. Yamamoto, T. Hirano et al., "Monitoring of singlet oxygen is useful for predicting the photodynamic effects in the treatment for experimental glioma," *Clinical Cancer Research*, vol. 12, no. 23, pp. 7132–7139, 2006.